Mean Climate and Circulation of Mock-Walker Simulations. Part 1: Comparison with Observations and Responses to Changing SST Gradients and Uniform Warming

Nicholas J. Lutsko[1], **Timothy W. Cronin**[2]

[1]Scripps Institution of Oceanography, University of California at San Diego, La Jolla, California

[2]Department of Earth, Atmospheric, and Planetary Sciences, Massachusetts Institute of Technology, Cambridge, Massachusetts

Key Points:

- Mock-Walker simulations compare favorably with the observed climate over the tropical Pacific, with some limitations
- Circulation changes dominate the responses to varying the SST gradient and to mean warming
- The model's climate sensitivity strongly increases when the SST gradient is reduced from a La Niña-like state to an El Niño-like state

Corresponding author: Nicholas Lutsko, `nlutsko@ucsd.edu`

Abstract

Improving understanding of the two-way interactions between clouds and large-scale atmospheric circulations requires modeling set-ups that can resolve cloud-scale processes, while also including representations of the forcings driving the circulations. In this study, we investigate the potential for mock-Walker simulations to help untangle these interactions, motivated further by a desire to clarify the mechanisms that relate changing sea-surface temperature (SST) patterns to variations in climate sensitivity. We assess the ability of mock-Walker simulations to reproduce the observed climate over the equatorial Pacific and investigate the model's responses to varying the SST gradient and to mean SST warming. A control simulation qualitatively reproduces many aspects of the climate seen in reanalysis and satellite data, though notable differences include the development of a double overturning cell, extreme dryness in the cold pool's upper troposphere and a substantially weaker long-wave cloud radiative effect. The model's responses to varying the SST gradient and to mean warming are strongly influenced by circulation changes; larger SST gradients accentuate the double-cell structure, while mean warming causes the lower circulation cell to strengthen and expand at the expense of the upper cell. Varying the SST gradient also strongly modulates the model's climate sensitivity, with a La Niña-like set-up having a low climate sensitivity and a strong negative cloud feedback, and an El Niño-like set-up having a high climate sensitivity and a strong positive cloud feedback.

1 Introduction

How clouds change in a warmer world remains the largest uncertainty in projecting future climate change under a given emission scenario [e.g., *Soden and Held*, 2006; *Forster et al.*, 2013; *Vial et al.*, 2013; *Schneider et al.*, 2017]. The reason for this is that cloud processes occur on scales that are too small for global climate models to resolve, so they must be represented by parameterizations, which suffer from both parametric and structural uncertainties as to whether they accurately represent the physics of convection and of cloud systems [*Randall et al.*, 2003; *Stevens and Bony*, 2013; *Schneider et al.*, 2017].

Uncertainty surrounding clouds and moist convection includes how they interact with their environment; improving our understanding of coupling between clouds and large-scale circulations has been identified as one of climate science's "grand challenges"

[*Bony et al.*, 2015]. Large-scale circulation cells are the main control on the spatial distribution of cloud-types in the tropics, as deep convective clouds are found in the rising branches of the Walker and Hadley circulations, and low clouds in the marine boundary layers beneath the descending branches. But the strengths and spatial structures of these circulation cells are strongly influenced by convective transports of heat, moisture and momentum, by the release of latent heat in moist convection, and by the reflection, absorption and emission of radiation by clouds. An improved understanding of the two-way interactions between clouds and large-scale atmospheric flows is needed to explain observed circulation patterns and cloud distributions, and to predict how these will change in a warmer world.

Untangling the interactions between clouds and circulation cells requires modeling set-ups that can resolve cloud-scale processes, while also including representations of the forcings driving the circulations. For example, some representation of the zonal sea-surface temperature (SST) gradient across the tropical Pacific [or, to ensure the system is energetically closed, of the ocean heat transport associated with it *Merlis and Schneider*, 2011] is required to study the coupling between clouds and the Walker circulation. Similarly, setting up a Hadley circulation requires rotation and meridional surface temperature gradients.

A number of recent studies have also documented how clouds respond to changing SST patterns, setting aside the question of how large-scale circulations mediate these responses. Past studies have examined how clouds respond to the oscillations of the zonal SST gradient in the equatorial Pacific during the El Niño-Southern Oscillation (ENSO) cycle [e.g., *Park and Leovy*, 2004; *Lloyd et al.*, 2012; *Lutsko*, 2018] and how changing SST patterns induce variations in the net climate feedback through their effects on cloud distributions. The latter includes studies of changing SST and cloud cover patterns over the historical period [*Andrews et al.*, 2018; *Silvers et al.*, 2018], and of the “pattern effect", whereby the evolution of SST patterns in high CO_2 simulations causes cloud feedbacks to vary over time, even if CO_2 concentrations are held fixed after an initial step increase [e.g., *Armour et al.*, 2013; *Meraner et al.*, 2013; *Andrews et al.*, 2015; *Ceppi and Gregory*, 2017; *Andrews and Webb*, 2018]. A related set of studies have calculated Green’s functions for the response of the cloud radiative effect to localized SST anomaly patches [*Zhou et al.*, 2017; *Dong et al.*, 2019]. Together, these different lines of investigation have shown that perturbing SSTs in the tropical west Pacific can induce large non-local cloud changes, which affect global climate through the top-of-atmosphere radiation budget. Conversely, perturbations in the tropical east Pacific tends to produce a more localized response. However, the dynamical mechanisms linking specific SST perturbations to their cloud responses have yet to be investigated in depth, partly because of the lack of idealized modelling set-ups which capture the relevant dynamics.

In this study, we examine the potential for "mock-Walker" simulations to help investigate these issues. Mock-Walker simulations use convection-permitting models (CPMs, also often called cloud-resolving models) in long-channel rectangular domains, with SSTs varying in the long dimension. Hence they include the zonal SST gradient needed to generate a realistic Walker-like circulation and grid resolutions sufficient to partially resolve convective processes. The mock-Walker set-up was first introduced by *Grabowski et al.* [2000], and we briefly review relevant subsequent literature in the following subsection. In this paper, we focus on comparing the climate of a control mock-Walker simulation with the observed atmosphere over the tropical Pacific, and on investigating the model's responses to varying the SST gradient and to increasing the mean SST. Our goals are to assess how well simulations reproduce the observed climate of the tropical Pacific and to document how simulations respond to SST perturbations.

In addition to potentially acting as a useful modelling framework for studying the interactions between SST perturbations, large-scale circulations and convection, we believe that mock-Walker simulations can act as a useful bridge between small-domain (widths of O(100 to 100s km)) CPM studies and the observed tropical atmosphere. Small-domain CPM simulations have provided many insights into the behavior of the tropical atmosphere and its response to warming [e.g., *Muller et al.*, 2011; *Muller and Held*, 2012; *Singh and O'Gorman*, 2013; *Romps*, 2014; *Wing and Emanuel*, 2014; *Seeley and Romps*, 2015; *Harrop and Hartmann*, 2016]; however, directly relating results from small-domain CPM simulations to the real tropical atmosphere is often complicated because the simulations are run over horizontally uniform SSTs, and do not generate large-scale flows.

Convection in CPM simulations also tends to cluster in a portion of the domain – a phenomenon known as convective self-aggregation [see *Wing*, 2019, for a recent review]. Convective self-aggregation is sensitive to the details of the model set-up and typically occurs for larger domains and coarser grids, so simulations run under slightly different conditions can produce very different climates [*Wing et al.*, 2018]. Global simulations of radiative-convective equilibrium (RCE), with parameterized clouds and convection, also exhibit self-aggregation [*Arnold and Randall*, 2015; *Coppin and Bony*, 2015; *Reed et al.*, 2015; *Pendergrass et al.*, 2016]. The mock-Walker set-up forces convection to cluster over the warmest SSTs, so there is less ambiguity about interpreting aggregation and about how simulations relate to the real tropical atmosphere; we thus view mock-Walker simulations a potentially useful complement to small-domain RCE simulations.

We have split the study into two parts. In Part 1, we begin by briefly reviewing previous mock-Walker studies in the following subsection, and then describe the model and simulations we have performed in section 2. The bulk of the paper consists of a comparison between a control mock-Walker simulation and the observed atmosphere over the tropical Pacific (section 3), and investigations of the model's response to varying the SST gradient, mimicking the perturbations of the El Niño-Southern Oscillation (section 4), and to increasing the mean SST, with both the control and the perturbed gradients (section 5). We briefly discuss the climate feedbacks and cloud responses in the various simulations in section 6, and finish with conclusions in section 7. In Part 2 we will provide interpretations of the dynamics seen in the simulations and also discuss modifications intended to make the model's climate more closely resemble the observed atmosphere over the tropical Pacific.

1.1 Previous mock-Walker studies

Past studies of mock-Walker simulations generally fall into three categories: *(1)* investigations of the mean states of mock-Walker simulations, *(2)* investigations of the variability of mock-Walker simulations, and *(3)* comparisons of mock-Walker simulations with simpler models.

(1) To our knowledge, the first study of mock-Walker simulations was by *Grabowski et al.* [2000], who found that 2D mock-Walker simulations with interactive radiation developed two vertically-stacked overturning cells (i.e., with two separate detached maxima in the longitude-height overturning streamfunction). We will refer to this as as a “double-cell" circulation. *Grabowski et al.* [2000] also showed that the double-cell could be eliminated by prescribing a fixed radiative cooling profile throughout the domain or by horizontally homogenizing radiative heating rates throughout the domain.

In follow-up work, *Yano et al.* [2002a] diagnosed the balances controlling the mean states of these circulations, and emphasized the importance of the vertical structure of the convective heating in determining formation of a single-cell or double-cell structure. Although this is relevant for interpreting the large-scale flow in our simulations, we have sought an explanation that requires no knowledge of the vertical structure of convective heating (to be discussed in Part 2). In a later study, *Liu and Moncrieff* [2008] examined the roles of surface friction, SST gradients, and horizontal contrasts in radiative cooling in regulating convection and circulation in mock-Walker simulations. A key result was that other factors besides SST gradients play important roles in determining the strength of the surface winds, which connect to the location and strength of convection – in contrast to the classical picture of *Lindzen and Nigam* [1987]. We discuss this further in Part 2.

(2) In another follow-up to the Grabowski et al study, *Yano et al.* [2002b] performed a linear perturbation analysis to understand the variability seen in their simulations. This analysis suggests that Walker circulations are linearly unstable, and spontaneously generate convectively-coupled gravity waves. Several other studies have noted that convectively-coupled waves cause quasi-periodic oscillations in mock-Walker simulations, corresponding to expansions and contractions of the convecting region. These oscillations generally occur on time-scales of ~2 days [*Grabowski et al.*, 2000; *Bretherton et al.*, 2006], though *Slawinska et al.* [2014] found longer time-scales of ~20 days. By analyzing specific events, *Slawinska et al.* [2014] showed that – in their set-up – the ~ 20-day variability is related to synoptic-scale systems, and that expansions and contractions of the convecting region involve different dynamics. The longer time-scales in their simulations are due to the use of a much larger domain – roughly 40,000km in the long dimension versus roughly 4000km in the other studies.

(3) Bretherton et al. [2006] compared CPM mock-Walker simulations with the Simplified Quasi-equilibrium Tropical Circulation Model (SQTCM), an idealized model of the tropical atmosphere based on quasi-equilibrium theory that includes simplified representations of cumulus convection and cloud-radiative feedbacks. The SQTCM was able to produce reasonable representations of the horizontal distributions of rainfall and horizontal energy fluxes in the mock-Walker simulations, however it was not able to capture the humidity distribution, the vertical structure of the circulation or the circulation's scaling with domain-size. *Kuang* [2012] mimicked the behavior of weakly-forced (i.e., weak SST gradient) mock-Walker simulations by combining linear response functions (to represent the

cumulus ensemble) with a parameterization of the large-scale flow based on the gravity wave equation. This simplified system was found to reproduce well the behavior of simulations with organized convection, including their sensitivity to moisture and temperature perturbations, but performed poorly as the convection became more disorganized. *Wofsy and Kuang* [2012] compared the horizontal precipitation and latent heating distributions in 2D mock-Walker simulations with prescribed radiative cooling, with a modified form of the theoretical Walker circulation model of *Peters and Bretherton* [2005]. A key modification by *Wofsy and Kuang* [2012] was the addition of a gustiness parameter, which allowed the theoretical model to capture the narrowing of the warm pool as the radiative cooling was increased.

In addition to these three categories, the most similar previous study to the present work is *Larson and Hartmann* [2003], who compared the climate of mock-Walker simulations run using the fifth-generation Pennsylvania State University-National Center for Atmospheric Research (PSU/NCAR) Mesoscale Model (MM5) with observations of the tropical Pacific, and also investigated the model's response to warming and to changing SST gradients. The MM5 model produced a reasonable simulation of the observed circulation, though it also produced a double-cell circulation. Increasing the SST gradient resulted in a more intense circulation and a narrowing of the convecting region, while increasing the mean SST but keeping the gradient fixed weakened the circulation slightly. Surprisingly, the outgoing long-wave radiation (OLR) was found to be roughly insensitive to the SST changes, because of compensating positive and negative feedbacks, whereas the short-wave radiation was found to be highly sensitive to SST changes, due to the model's low cloud response. However, the finest grid-spacing used by Larson and Hartmann was 60km – far too coarse to resolve cloud processes. We also recently used 2D mock-Walker simulations as part of an investigation of the changes in precipitation efficiency with warming, finding that the precipitation efficiency is high in regions of deep convection and low in the stratus clouds over the cold pool [*Lutsko and Cronin*, 2018].

Finally, a number of studies have used RCE simulations in domain geometries akin to mock-Walker set-ups, but over uniform SSTs, to explore mechanisms that lead to organization of convection, the strength of large-scale circulations, and how cloud and rain distributions change with warming [*Grabowski and Moncrieff*, 2001, 2002; *Stephens et al.*, 2008; *Posselt et al.*, 2008, 2012; *Wing and Cronin*, 2016; *Cronin and Wing*, 2017]. Although the large-scale circulations in these simulations are weakly constrained compared to mock-Walker simulations, certain properties of observed large-scale tropical flows can be reasonably reproduced, such as the distributions of large-scale mid-tropospheric vertical motion [*Cronin and Wing*, 2017] and humidity variability [*Holloway et al.*, 2017], and the diabatic processes that favor and disfavor convective aggregation over a range of length scales [*Beucler et al.*, 2019]. These uniform-SST long-channel simulations provide another useful stepping stone for relating small domain CPM studies to the observed tropical atmosphere [see also *Wing et al.*, 2018].

2 Model, Simulations and Data

2.1 Model description

All simulations were performed with version 6.10.8 of the System for Atmospheric Modeling (SAM, *Khairoutdinov and Randall* [2003]). This model solves the anelastic continuity, momentum and tracer conservation equations, and its prognostic thermodynamic variables are liquid/ice water static energy, total nonprecipitating water (vapor, cloud water and cloud ice) and total precipitating water (rain, snow and graupel).

The simulations were conducted without rotation and with fixed SSTs, and used a vertical grid with 64 levels, starting at 25m and extending up to 27km. The vertical grid spacing increases from 50m at the lowest levels to roughly 1km at the top of the domain. A sponge layer damps the flow at the top of the domain, and subgrid-scale fluxes are parameterized using Smagorinsky's eddy diffusivity model. A variable time-step was used, with maximum interval 10s, and radiative fluxes were calculated every 40 time-steps. The incoming solar radiation was fixed at 650.83Wm^{-2}, with a zenith angle of 50.5° [*Tompkins and Craig*, 1998], producing a net insolation close to the tropical-mean value, and the simulations were initialized with a small amount of white noise added to the temperature field near the surface to initiate convection.

2.2 Simulations

We focus on 3D simulations conducted in a domain of length L = 12,288km in the x-direction and width 96km in the y-direction. SSTs are prescribed to a profile that is sinusoidal in x, with a wavelength of $2L$ such that the SST varies over half a wavelength within the domain, and a peak-trough amplitude of ΔT: $\mathrm{SST}(x) = T_0 + (\Delta T/2)\cos(\pi x/L)$. The domain is periodic in y, while vertical walls are placed on either side of the domain

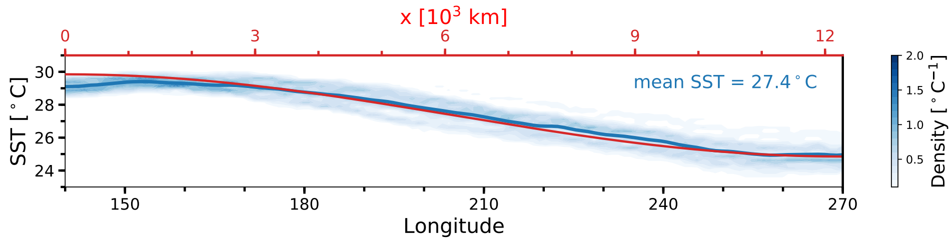

Figure 1. Monthly SST distributions, averaged from 5°S to 5°N, in the tropical Pacific (blue contours). Data are taken from the HADISST1 dataset, available from https://www.metoffice.gov.uk/hadobs/hadisst/, and span the period 1950-2017. The thick blue line shows the mean of the PDF at each longitude, and the regional-mean sea surface temperature is 27.4°C. The red line shows the SST profile in the control mock-Walker simulation. The bottom y-axis corresponds to the HADISST data, and spans a distance of roughly 14,430km, while the scale of the top y-axis corresponds to the SAM domain and spans 12,288km. So the bottom axis is stretched by approximately 17% compared to the top axis.

in x, with the warmest SSTs located near one wall and the coldest SSTs near the other wall. The horizontal grid-spacing is set to 3km in all simulations. Tests showed that using a domain with walls has a minor effect on the flow in the model compared to using a doubly-periodic domain of length $2L$ = 24,576km, which would allow the SST to vary over a full wavelength, with primary differences localized to within about 100km of the walls (not shown). We used smaller domains with walls in order to reduce computational burden. All simulations were run for 200 model days, with averages taken over the last 100 days.

Our control simulation used a mean SST T_0 = 300.5K, with a 5K difference (ΔT) between the warmest and coldest SSTs, creating a comparable SST gradient to the equatorial Pacific (see Figure 1). This simulation used the single-moment SAM microphysics scheme [*Khairoutdinov and Randall*, 2003] and the CAM radiation scheme [*Collins et al.*, 2006]. From this starting point, simulations were conducted with T_0 increased by 2K and with ΔT increased and decreased by 1K, mimicking extreme states of the El Niño-Southern Oscillation (ENSO). We have also run a strong cooling (T_0 = 290K) and a strong warming (T_0 = 310K[1]) experiment. A complete list of the SAM simulations is given in Table 1.

[1] In this simulation the vertical grid included 75 levels and extended up to 36km.

Table 1. List of 3D mock-Walker simulations performed with SAM.

simulation name	mean SST [K]	ΔT [K]
control	300.5	5
El Niño	300.5	4
La Niña	300.5	6
+2K warming	302.5	5
+2K warming-El Niño	302.5	4
+2K warming-La Niña	302.5	6
strong cooling	290	5
strong warming	310	5

2.3 Reanalysis and observational data

Meteorological data are taken from the ERA-Interim dataset [*Dee et al.*, 2011] and top-of-atmosphere (TOA) radiative fluxes from the Clouds and the Earth's Radiant Energy System (CERES) dataset to compare with the simulations. The ERA-Interim grid has ~0.75° resolution in latitude and longitude, and we have used monthly-mean data for the years 1979 to 2013. The CERES data comprise all-sky and clear-sky TOA fluxes, from which we have calculated the cloud radiative effect (CRE) as all-sky fluxes minus clear-sky fluxes. Data are taken for the period March 3rd 2003 to October 10th 2013, and interpolated onto a $1° \times 1°$ grid.

To compare with the mock-Walker simulations we consider the atmosphere above a section of the equatorial Pacific, from 140°E to 270°E and meridionally-averaged from 5°S to 5°N. This is comparable to the length of the mock-Walker domain (~14,430km compared to 12,288km) and includes both a maximum and a minimum in the climatological SST profile (Figure 1).

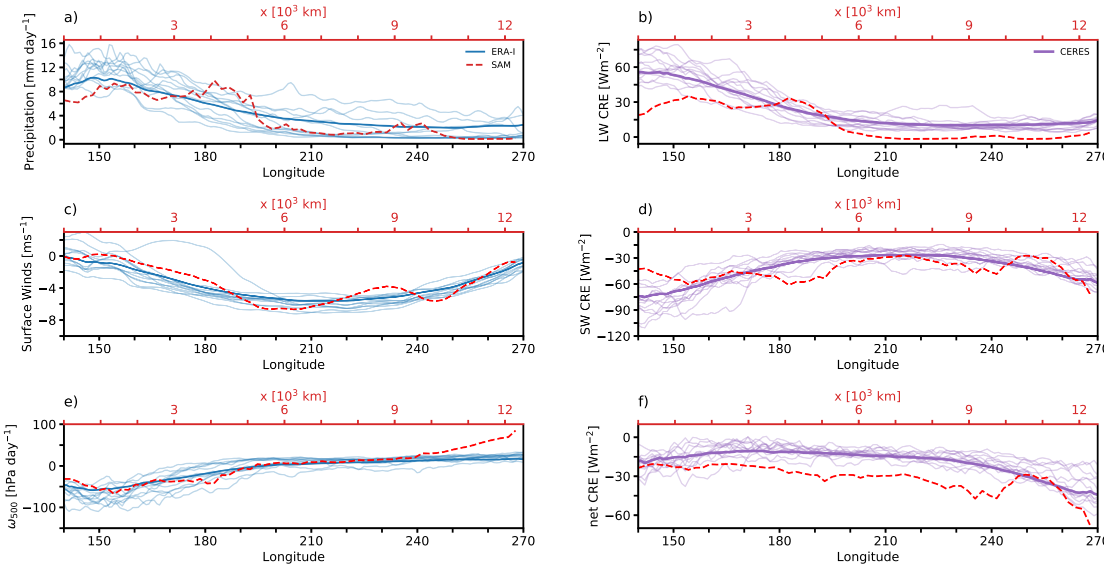

Figure 2. a) Climatological precipitation over the equatorial Pacific, averaged from 5°S to 5°N, for the ERA-Interim data (thick blue line) and precipitation averaged over the last 60 days of the control 3D SAM simulation (dashed red line). The thinner blue lines show monthly-means of equatorial Pacific precipitation for the year 2006, which was a neutral ENSO year. b) Climatological LW CRE over the equatorial Pacific, averaged from 5°S to 5°N, for the CERES data (thick purple line) and LW CRE averaged over the last 60 days of the control 3D SAM simulation (dashed red line). The thinner purple lines show monthly-mean LW CRE for the year 2006. c) Same as a) but for the near-surface zonal winds. d) Same as b) but for the SW CRE. e) Same as a) but for the ω_{500} velocities. f) Same as b) but for the net CRE. Note that in all panels the scale of the bottom y-axis corresponds to the reanalysis and satellite data, while the scale of the top y-axis corresponds to the SAM domain.

3 Comparing the Control Simulation to Observations

3.1 Zonal profiles

We begin by comparing zonal profiles of meteorological variables and CREs from the control simulation with reanalysis and satellite data. The CRE comparison is of particular interest, since one of our primary aims is to assess the utility of the mock-Walker set-up for studying cloud feedbacks under warming.

There are a number of similarities between the mock-Walker simulation and the ERA-Interim data. The maximum precipitation in the simulation is comparable to the reanalysis data, though the sharp simulated transition from high to low precipitation rates resembles individual observed months more than the long-term ERA-Interim climatology (Figure 2a). A secondary simulated peak in precipitation near $x = 9{\times}10^3$km is not seen in observations. Simulated surface winds compare closely in magnitude and overall shape to reanalyis winds, but show more than one local maximum in speed, in contrast to the reanalysis data (Figure 2c). Higher up, the simulated ω_{500} compares well to the reanalysis except over the far-eastern cold pool where the simulated descent is far stronger; we hypothesize this occurs because the simulated domain is closed, so mass must be conserved, whereas the reanalysis data are averaged over an open domain at latitudes of mean ascent.

The simulated long-wave (LW) CRE shows broadly similar structure to the CERES climatology in that both are stronger over the warm pool and weaker over the cold pool (Figure 2b), but the magnitude of simulated LW CRE averages only half that seen in observations. The short-wave (SW) CREs in CERES observations and the control simulation have comparable magnitudes (Figure 2d), but the simulated SW CRE shows additional minima near precipitation maxima at $x = 4 \times 10^3$km and $x = 9 \times 10^3$km, as well as near the eastern boundary of the domain. As with precipitation, more maxima and minima lead simulated SW CRE patterns to compare better with monthly observations than with climatology, but even on monthly time-scales the simulated LW CRE is biased low.

These discrepancies in the LW and SW CRE lead to substantial differences in the net CRE profiles between simulations and observations (Figure 2f): net CRE is biased low across most of the middle of the domain and also the eastern boundary by $\sim$ 20 Wm^{-2}. We note, however, that the simulated SW CRE may be overestimated in magnitude, as we use a daytime-weighted zenith angle, rather than an insolation-weighted zenith angle [*Cronin*, 2014]. With a global-mean cloudscape, this would give an overestimate of the SW CRE's magnitude of about 10 Wm^{-2}, and would partly compensate for the bias in the net CRE.

3.2 Warm pool and cold pool climates

The SST contrast across the simulation domain creates a “warm pool" region in the western part and a “cold pool" region in the eastern part of the domain. To compare the climates of these regions with observations over the West Pacific warm pool and east Pacific cold pool, Figure 3 shows vertical profiles of temperature, relative humidity, moist

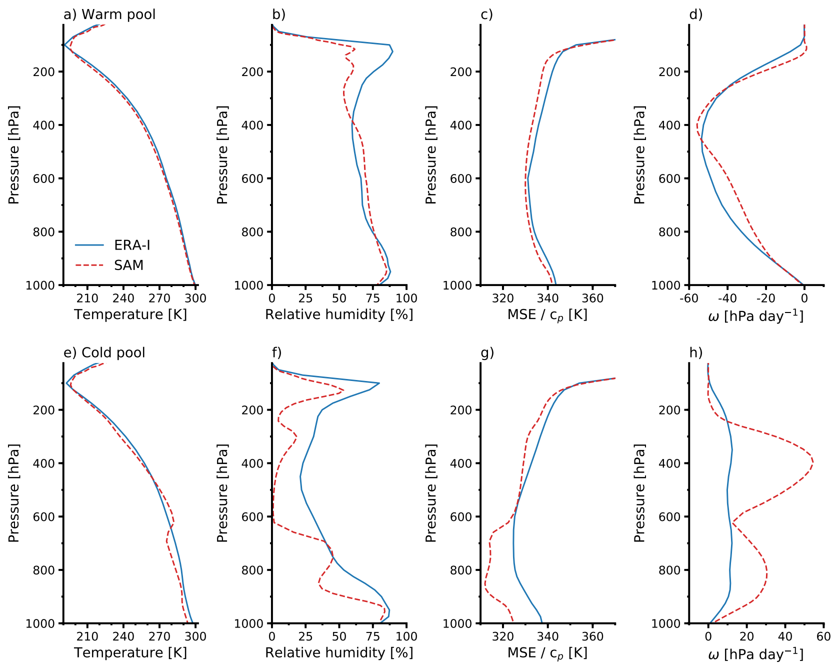

Figure 3. a) Vertical profiles of temperature in the warm pool of the ERA-Interim data (solid blue, averaged over 140-160°E and 5°S-5°N) and in the warm pool region of the control simulation (dashed red, averaged over x = 1-3×10^{3}km). b) Same as a), but showing vertical profiles of relative humidity, averaged over the same regions. c) Same as a), but showing vertical profiles of moist static energy, averaged over the same regions. d) Same as a), but showing vertical profiles of the vertical pressure velocity, averaged over the same regions. e) Vertical profiles of temperature in the cold pool of the ERA-Interim data (solid blue, averaged over 240-260°E and 5°S-5°N) and in the cold pool region of the control simulation (dashed red, averaged over x = 10-12×10^{3}km). f) Same as e), but showing vertical profiles of relative humidity, averaged over the same regions. g) Same as e), but showing vertical profiles of moist static energy, averaged over the same regions. h) Same as e), but showing vertical profiles of the vertical pressure velocity, averaged over the same regions.

static energy (MSE = $c_pT + L_vq_v + gz$[2]) and vertical pressure velocity from reanalysis (blue lines) and the control simulation (dashed red lines). The top panels show averages taken over the warm pool (150-170°E and 5°S-5°N in reanalysis and x = 1-3×10^{3}km in the simulation), and the bottom panels show averages taken over the cold pool (240-260°E

[2] c_p is the heat capacity of dry air, T is temperature, L_v is the latent heat of vaporization of water, q_v is the specific humidity, g is Earth's gravitational acceleration and z is height

and 5°S-5°N in reanalysis and x = 10-12×10^3km in the simulation). Regions are also indicated in Figure 4.

Warm-pool profiles compare much more tightly between simulations and reanalysis than do cold-pool profiles. Over the warm pool, simulated temperature profiles closely match reanalysis (Figure 3a), relative humidities are close (Figure 3b[3]), MSE profile shapes are similar but biased slightly low in simulations due to a slightly cooler troposphere (Figure 3c), and ascent velocities are comparable but with a more top-heavy structure in the control simulation (Figure 3d; for ease of discussion, we will refer to ascent "maxima" even though the pressure velocities are negative over the warm pool). In reanalysis data, the vertical velocity peaks at around 500hPa, with faster ascent in the lower troposphere than the simulation.

Over the cold pool, simulated thermodynamic and dynamic profiles differ much more from ERA-Interim data. The simulation is substantially colder in the lower troposphere, and there is a strong temperature inversion at about 650hPa that is not seen in the reanalysis (Figure 3e; note that the cold pool of the simulation also has a weaker boundary layer-capping inversion near 900hPa). The cold pool of the simulation is drier than the reanalysis data at almost all levels, with the relative humidity approaching 0% in the mid-troposphere. Reflecting these differences, the MSE is much lower (20-25K) in the lower troposphere of the simulation than in reanalysis. Above the inversion the simulated MSE is closer to the observed MSE profile, but differences as large as 8K remain. The descent profile over the cold pool of the simulation has two maxima and much larger magnitude than reanalysis (recall that the reanalysis data are taken from latitudes of mean ascent); the implied double-celled flow structure is discussed more below.

Simple models of the Walker circulation often represent ascent and descent with a single vertical mode [the first baroclinic mode, e.g., *Bretherton and Sobel*, 2002; *Peters and Bretherton*, 2005; *Wofsy and Kuang*, 2012; *Emanuel*, 2019]. That the ascent in the warm pool region has a single maximum and the descent in the cold pool region has two maxima suggests that such simple theories will not capture the behavior of our control simulation. Furthermore, the large differences in the MSE profiles across the domain

[3] By default, SAM outputs relative humidity calculated over liquid water only. However, in this manuscript relative humidities are reported over liquid water for temperatures ≥0°C and over ice for temperatures <0°C.

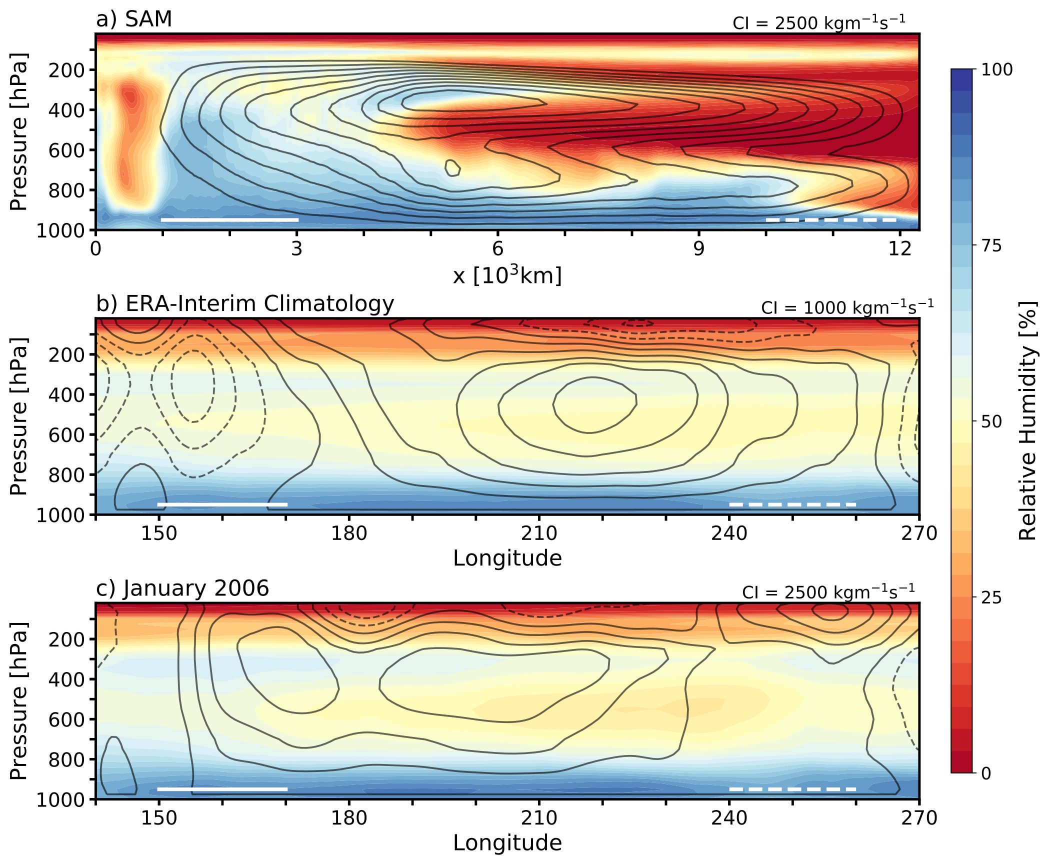

Figure 4. a) Mean relative humidity (colored contours) and streamfunction (black contours) for the control SAM simulation. b) Same as panel a) but for the ERA-Interim data, averaged over 1979-2012, and with the streamfunction calculated using the divergent zonal-wind. c) Same as panel b) for the ERA-Interim data for January 2006. The contour intervals for the streamfunctions are indicated above the panels, with solid contours indicating clockwise flow and dashed contours indicating counterclockwise flow. The solid white and dashed white lines in each panel indicate the warm pool and cold pool regions, respectively, in the simulation and the observational data.

suggest that energy transports can not be diagnosed solely from vertical velocity profiles [e.g., *Back and Bretherton*, 2006; *Inoue and Back*, 2015]. Thus, a full theory for the circulation and energy transport in this mock-Walker set-up must consider at least two modes of variability in vertical velocity, horizontal advection across MSE gradients, and substantial variation of the temperature and humidity profiles between warm-pool and cold-pool regions.

3.3 Overturning circulation

We finish this section by comparing the simulated overturning circulation with that seen in reanalysis. Figure 4 shows the streamfunctions (black contours) and the relative humidity (colored contours) of the control simulation (panel a), of the climatological ERA-Interim data (panel b) and of a representative month, January 2006 (panel c). The streamfunctions are calculated as $\frac{1}{g}\int_{1000hPa}^{p}\bar{u}(p',\phi)dp'$, where u is the zonal wind from the simulation or the divergent component of the zonal wind (u_D) from the reanalysis data [*Schwendike et al.*, 2014], and an overbar denotes a y-direction or meridional average[4].

Flows in the three panels show a few broad similarities – ascent over the warm pool (the West Pacific), outflow in the upper troposphere, descent over the cold pool (the East Pacific) and a decrease in the upper tropospheric relative humidity moving eastward from the warm pool to the cold pool[5] – but several differences are also apparent. First, the simulated mid- and upper-troposphere is much drier than the reanalysis over the cold pool, with relative humidities of less than 10%. In reanalysis from January 2006, there is a dry patch in the mid-troposphere, but even there the lowest relative humidities are ~30%. This suggests that transient tropical waves or meridional moisture transports not simulated by the model may play a crucial role in moistening the middle and upper troposphere over the cold pool.

A second major difference is that the flow in the SAM simulation has a double-cell structure, particularly over the cold pool, whereas reanalysis shows a single overturning cell in both climatology and individual months. In the simulation a single overturning cell, centered at around 400hPa, occupies most of the upper troposphere, while two cells are visible in the lower troposphere. One cell connects the warm pool and the cold pool, with ascent over the warm pool and descent between roughly x = 6 - 8$\times10^3$km, and there is a second overturning cell over the cold pool, with shallow convection near x = 9$\times10^3$km, aligned with the secondary precipitation and SW CRE maxima (Figure 2). We

[4] Note that the ERA-Interim data are averaged over a limited sector, so the circulation does not necessarily conserve mass.

[5] We are unsure what causes the dry quiescent region over the western edge of the warm pool in the SAM simulation. It may be a transient feature, which would be smoothed out in longer simulations, or it could be caused by the presence of a wall in our simulations or the lack of background zonal flow. Note that this feature is not present in all of the simulations (see Figures 5 and 8).

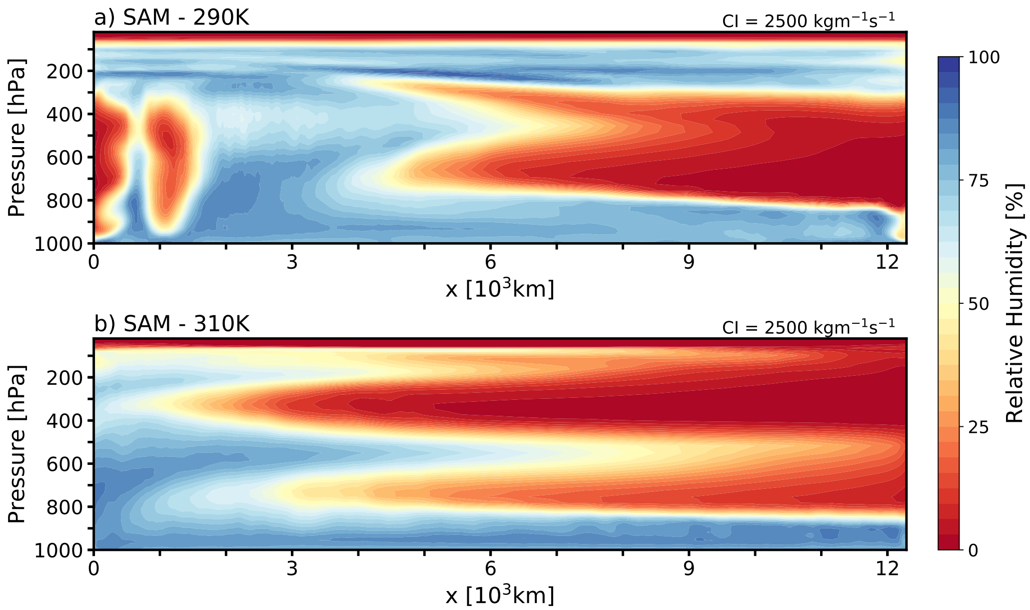

Figure 5. a) Mean relative humidity (colored contours) and streamfunction (black contours) for the SAM simulation with a mean SST of 290K. b) Same as panel a) but for the SAM simulation with a mean SST of 310K. The contour intervals for the streamfunctions are indicated above the panels, with solid contours indicating positive (clockwise) flow and dashed contours indicating negative flow.

have been unable to find any months in reanalysis data which exhibit such a clear double-cell vertical structure as seen in the simulation.

We recently found a flow-transition in 2D mock-Walker simulations from a single vertical cell at relatively cold (<~300K) SSTs to a double cell at warmer SSTs (>~300K) [*Lutsko and Cronin*, 2018]. This transition is reproduced in the 3D simulations, as for a mean SST of 290K there is a single overturning cell and for a mean SST of 310K there is a clear double cell, with a strong outflow from the convecting region at around 500hPa (Figure 5). As in the 2D simulations, the transition occurs for a mean SST of $T_0 \sim 300$K. In part 2 of our study of mock-Walker simulations, we provide explanations for this transition, including why it occurs for $T_0 \sim 300$ and also why double-cells are rarely seen over the equatorial Pacific in the reanalysis data.

3.4 Summary

To summarize this section, the mock-Walker simulation qualitatively reproduces several aspects of the equatorial Pacific climate, as represented by the reanalysis data, includ-

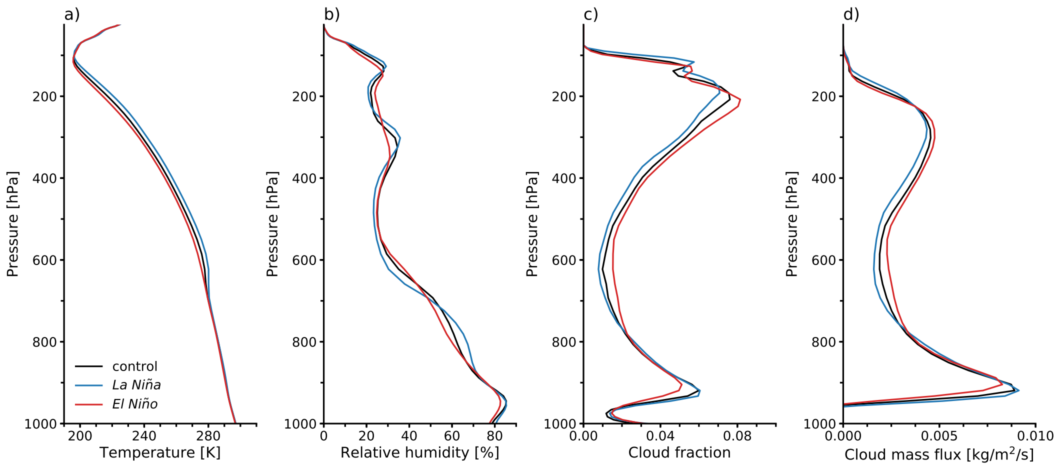

Figure 6. a) Profiles of horizontal-mean temperature from the control mock-Walker simulation (black), the La Niña simulation (blue) and the El Niño simulation (red). b) Same as a) but for the relative humidity. c) Same as a) but for the cloud fraction. d) Same as a) but for the convective mass flux.

ing the zonal profiles of precipitation, surface winds and LW CRE, and the temperature and humidity profiles over the warm pool. However there are also major differences, including an overall reduction in cloud cover (leading to a smaller LW CRE than observed), much lower humidities in the middle and upper troposphere over the cold pool region of the simulation and the development of a double overturning cell.

4 Responses to Varying the SST Gradient

4.1 Horizontal-mean climate

Increasing and decreasing the SST gradient allows us to investigate the model's response to La Niña-like and El Niño-like perturbations, respectively. We begin by examining how this affects the horizontal-mean climates of the model. Horizontally-averaged temperature profiles in the three simulations are very similar up to 700hPa, where the La Niña profile has an inversion and then remains warmer than the other two simulations throughout the middle and upper troposphere (Figure 6a). The control simulation also has an inversion, near 650hPa, above which it is warmer than the El Niño simulation. Both inversions coincide with reductions in relative humidity (Figure 6b), with the stronger La Niña inversion having a larger humidity drop. The horizontally-averaged temperature of the El Niño simulation shows no inversion, but relative humidity still declines from roughly 45% at 700hPa to roughly 30% at 550hPa. At higher altitudes there are two rel-

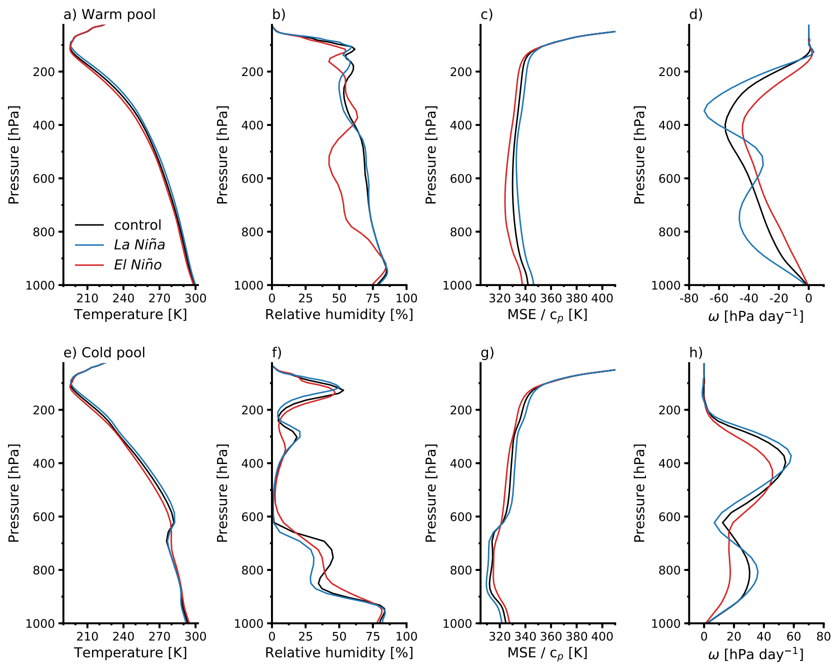

Figure 7. As in Figure 4, but comparing the control SAM simulation (black curves) with the La Niño simulation (blue curves) and the El Niño simulation (red curves).

ative humidity maxima in all simulations (near 300hPa and 150hPa), but the maxima are less pronounced in the El Niño simulation.

The cloud fractions and mass fluxes above the boundary layer are smaller in the La Niña simulation and larger in the El Niño simulation (Figure 6c and d), while the low cloud fraction is slightly larger in the La Niña simulation than in the control simulation, and substantially smaller in the El Niño simulation. The relative humidity is also lower in the boundary layer of the El Niño simulation (i.e., below 900hPa). In the upper troposphere, cloud fraction peaks occur at higher altitudes in the La Niña simulation and lower altitudes in the El Niño simulation.

4.2 Warm pool and cold pool climates

Warm pool and cold pool climates show some progressive changes and some abrupt shifts as the SST contrast is varied (Figure 7). Temperatures in the warm pool and well above the inversion in the cold pool follow moist adiabats (Figure 7a,e) with the La Niña profile warmer and the El Niño profile cooler than the control profile. This reflects differences in warm pool SSTs and suggests that temperatures above the cold pool inversion, but not below it, are set by convection over the warm pool. The El Niño simulation is substantially drier than the control simulation in the mid-troposphere over the warm pool, but has both positive and negative humidity anomalies over the cold pool (Figure 7b,f). The La Niña simulation, on the other hand, is substantially drier than the control simulation in the low and mid-troposphere over the cold pool but has both positive and negative anomalies over the warm pool (Figure 7b,f). Together with temperature differences, these humidity differences lead to similar MSE profile shapes over the warm pool (Figure 7c), but higher MSE values for the La Niña simulation and lower values for the El Niño simulation. Over the cold pool, the lower-troposphere MSE minimum is least pronounced for the El Niño simulation and most pronounced for the La Niña simulation (Figure 7g).

Circulation patterns show some abrupt shifts as the SST contrast is varied (Figure 7d,h). Two maxima appear in the La Niña ascent profile – one at 350hPa and one at 800hPa – and the ascent is generally stronger than in the control case. The double-cell subsidence pattern in the cold pool mostly disappears in the El Niño simulation, with nearly uniform and weaker descent than the control simulation in the lower troposphere above the boundary layer. Warm-pool ascent in the El Niño simulation and cold-pool subsidence in the La Niña simulation mostly appear to be dampened and amplified versions, respectively, of the control profiles. Overall, these vertical velocity profiles suggest a marked shift towards a domain-spanning double-cell circulation for increased SST contrast, and an elimination of the double-cell structure for weakened SST contrast.

4.3 Overturning circulations

The overturning circulations of the control simulation and of the La Niña simulation are similar (Figure 8a,b), but ascent is stronger and more confined and the double-cell structure more prominent in the La Niña simulation. The narrower ascent in the La Niña simulation is also apparent from the zonal profile of precipitation (Figure 9), and in the larger subsidence fraction in the La Niña simulation relative to the control simulation (0.64 compared to 0.58). In contrast to the overturning circulations of the La Niña and control simulations, a single overturning cell occupies most of the domain in the El Niño simulation (Figure 8c), with a shallow secondary cell over the cold pool, as also seen in the control simulation. The flow is substantially weaker than in the other two simulations, and convection over the cold pool produces a second precipitation maximum on the west-

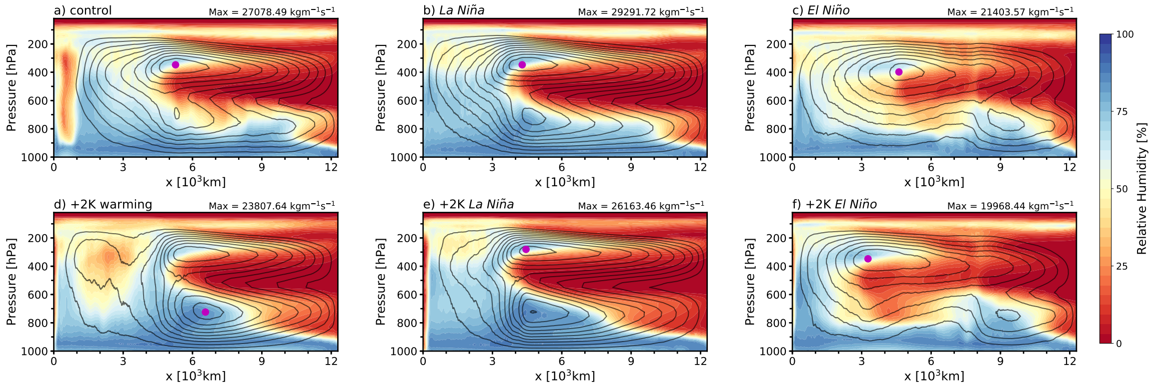

Figure 8. Mean relative humidity (colored contours) and streamfunction (black contours) for the control SAM simulation (a), the La Niña simulation (b), the El Niño simulation (c), the +2K simulation (d), the +2K-La Niña simulation (e) and the +2K-El Niño simulation (f). The contour interval for the streamfunctions are the same in each panel, with solid contours indicating positive (clockwise) flow and dashed contours indicating negative flow. The data from the control simulation are repeated from Figure 3a for ease of comparison. The magenta markers show the locations of the streamfunction maxima, and their magnitude is indicated above each panel. The contour interval in all panels is $2500\mathrm{kgm^{-1}s^{-1}}$.

ern edge of the cold pool that is comparable to the maximum over the warm pool, and much stronger than in the control simulation (Figure 9). The subsidence fraction in the El Niño simulation is comparable to the control simulation (0.58), but relative humidities in the middle of the domain (between roughly x = 4 - 8×10^{3}km) are larger than in the control and La Niña simulations.

4.4 Summary

Overall, the climate of the La Niña simulation resembles the control simulation more than the El Niño simulation does. Compared to the control simulation, the La Niña simulation shows similar warm pool and cold pool temperature and moisture profiles, and a broadly similar large-scale circulation. Main differences include domain-average profiles that are warmer and drier, with less cloud cover (Figure 5), a more pronounced double-cell flow structure (Figure 8), more concentrated and stronger ascent, and a stronger overturning circulation overall. In the horizontal mean, the El Niño simulation is colder than the control simulation, with more cloud cover above the boundary layer. Although there is a shallow secondary overturning cell over the cold pool of this simulation, the circulation

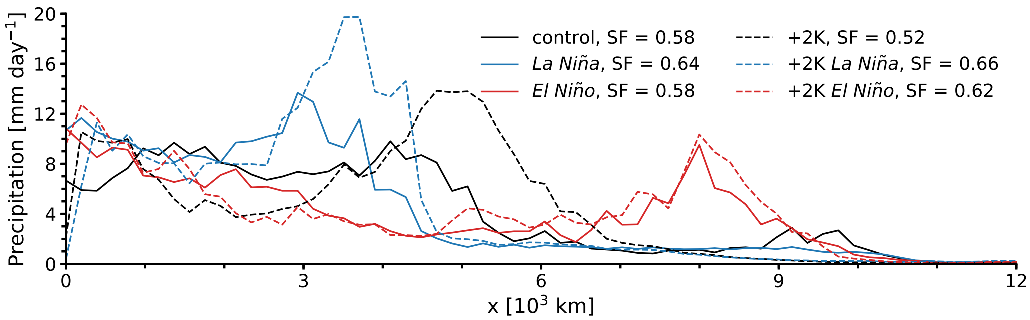

Figure 9. Zonal profiles of precipitation in the mock-Walker simulations, averaged over the y dimension (the narrow dimension). The subsidence fraction SF is given in the legend for each simulations, and is defined as the fraction of the domain with $\omega > 0$, averaged over 700-400hPa.

is dominated by a single overturning cell, and the distinction between the upper and lower circulation cells is less well defined than in the other two simulations (i.e., the temperature inversion over the cold pool is much weaker). The circulation is also substantially weaker in the El Niño simulation – consistent with *Larson and Hartmann* [2003], who found that the overturning circulation in their coarse-resolution mock-Walker simulations weakened as the SST gradient was decreased.

5 Responses to Uniform Warming

5.1 Domain-mean climate

In our final set of comparisons, we investigate how the model's climate responds to increasing the mean SST by 2K, in simulations with the control, enhanced and reduced SST contrasts. The control and La Niña simulations respond similarly to warming, including sharp warming minima near 600hPa (Figure 10a) which reflect changes in the circulation: in both cases the lower circulation cells expand vertically (Figure 8d,e), so that cold pool temperature inversions shift to higher altitudes, producing warming minima when comparing to control simulations. The La Niña case warms more than the control case throughout most of the troposphere, likely because upper-tropospheric warming is amplified for a warmer moist adiabat. The warming in the +2K-El Niño simulation is roughly moist adiabatic, with a maximum near 250hPa, and no clear warming minimum associated with a rising inversion.

In all three cases the boundary layer relative humidity increases (Figure 10b), and above this there are alternating regions of moistening and drying, which partly reflect the circulation changes: the lower cell expanding vertically and the upper cell contracting and shifting to higher altitudes. For instance, the relative humidity increases between 700hPa and 500hPa in the control and La Niña cases, as the outflow of moist air from the convecting region at the top of the lower circulation cell moves to higher altitudes. The relative humidity decreases below 700hPa. In the El Niño case the relative humidity increases between 900hPa and 700hPa in the +2K simulation, in contrast to the other two set-ups, but above these heights the relative humidity changes have a similar vertical structure to the control and La Niña cases, alternately moistening and drying, though the changes are substantially smaller in the El Niño set-up.

In all three cases the boundary layer relative humidity increases (Figure 10b), and above this there are alternating regions of moistening and drying, which partly reflect the circulation changes: the lower cell expanding vertically and the upper cell contracting and shifting to higher altitudes. For instance, the relative humidity increases between 700hPa and 500hPa in the control and La Niña cases, as outflow of moist air from the convecting region at the top of the lower circulation cell moves to higher altitudes. In the +2K El Niño simulation the relative humidity changes show similar alternation between moistening and drying, but the magnitude of changes is muted.

Low clouds ($\leq$850hPa) stay at roughly the same pressure with warming, while the mid- and upper-tropospheric clouds remain at roughly constant temperatures, so we plot cloud changes in both vertical coordinates (Figure 10c, d). The low cloud cover near the top of the boundary layer increases with warming in all three simulations (Figure 10c), but surface maxima in cloud cover (Figure 6c), likely fog, decrease in warmer climates. High cloud fraction decreases in all simulations at sufficiently low temperatures, but there are moderate increases in some high clouds for the control and La Niña simulation (Figure 10d).

5.2 Overturning circulations

As discussed earlier, in the +2K experiments with the control and La Niña SST gradients, the lower circulation cells strengthen and expand vertically (Figure 8d,e). For the control case the two shallow circulation cells merge with warming, creating a single lower cell that spans most of the domain (Figure 8a,d), and the streamfunction maximum shifts into the lower troposphere. Precipitation maxima in both the control and La Niña cases intensify by $\sim$ 50% and shift slightly east with warming (Figure 9). This suggests that convection becomes more concentrated, but changes in subsidence fraction are mixed, increasing in the La Niña set-up from 0.64 to 0.66 but decreasing in the control set-up from 0.58 to 0.52. In contrast, the flow in the El Niño simulations is less obviously altered in structure by warming (Figure 8c,f), and changes in precipitation maxima are less pronounced (Figure 9), although the subsidence fraction does increase from 0.58 to 0.62. Overall, these results caution against using subsidence fraction as a standalone metric of overturning circulation changes, as the notable circulation changes seen here do not manifest in a consistent way in subsidence fraction changes.

5.3 Responses over the cold pool

The responses of the warm pools in the +2K experiments are similar, as the temperatures shift to warmer moist adiabats (not shown), while changes over the cold pool are more varied (Figure 11). In all three set-ups cold pool temperatures increase and inversions move to higher altitudes, such that the original control and La Niña simulations are actually warmer at 600hPa than the +2K simulations. The control and La Niña set-ups also dry markedly in the lower troposphere: relative humidities between 850hPa and 600hPa are roughly halved by a 2K warming (Figure 11b and e). In contrast, the El Niño set-up moistens with warming in most of the lower troposphere (Figure 11h). All three simulations dry with warming in the upper troposphere, but with differing vertical structures: the control and La Niña cases dry above 200 hPa and moisten near 250 hPa, suggestive of an upwards shift of a cloud layer near 300 hPa, but the El Niño simulation shows moistening and an upward shift of a higher peak in relative humidity around 100hPa.

The subsidence profiles in the control and La Niña set-ups shift upwards by ~50-100hPa with a 2K warming, with descent strengthening in the lower cell but weakening in the upper cell (Figure 11c, f). In the El Niño set-up profiles shift much less in pressure and weaken throughout the troposphere with warming, with a hint of a more pronounced maximum in lower-tropospheric subsidence emerging as subsidence weakens more at 700hPa than at lower altitudes.

Table 2. Cess feedbacks, clear-sky Cess feedbacks and net CRE changes for the three sets of mock-Walker simulations. The Cess feedback are calculated as the change in net top-of-atmosphere radiation divided by 2K.

SST gradient	Cess feedback [Wm^{-2}/K]	Clear-sky Cess feedback [Wm^{-2}/K]	Δnet CRE / ΔT_s [Wm^{-2}/K]
control	-1.47±0.78	-1.47±0.22	0.01±0.57
La Niña	-3.49 ±1.09	-1.51±0.88	-1.97 ±0.71
El Niño	-0.49±0.43	-1.49±0.39	1.00±0.34

5.4 Summary

The responses of the control and La Niña set-ups to warming are dominated by the circulation response, particularly the expansion and strengthening of the lower circulation cells, and the contraction of the upper cells. Circulation changes dominate the vertical profile of temperature change, regulate changes in humidity and in cloud cover, and lead to $\sim$ 50% increases in the precipitation maxima near the edge of the warm pool for only 2K of surface warming. The response in the El Niño set-up is less mediated by the circulation, which weakens but retains a similar structure. As a consequence, profiles of temperature change are smoother, humidity changes are muted, and precipitation maxima change less in amplitude. Another notable difference is that the relative humidity increases in the lower troposphere of the El Niño set-up with warming, whereas the lower troposphere dries in the other two set-ups. Finally, there is a large increase in cirrus cloud cover over the cold pool in this set-up, compared to a reduction in the other two set-ups.

6 Feedbacks and Cloud Responses

"Cess" climate feedbacks (λ) can be calculated for the three configurations as the change in net top-of-atmosphere radiative flux R between the original and +2K experiments, divided by 2K: $\lambda = \frac{R_{+2K} - R_0}{2K}$ [*Cess and Potter*, 1988]. This gives feedbacks of λ = -1.47±0.78 Wm^{-2}/K for the control SST gradient, λ = -3.49±1.09 Wm^{-2}/K for the enhanced La Niña gradient and λ = -0.49±0.43 Wm^{-2}/K for the reduced El Niño gradient[6]. This suggests that climate sensitivity varies by a factor of ~6 across the simulations, with the El Niño set-up having a very high sensitivity (higher than any climate model we know of) and the La Niña set-up having a very low climate sensitivity (lower than any climate model we know of). As clear-sky feedbacks are similar across the different set-ups (Table 2), these variations in sensitivity are largely due to differences in the cloud feedback: the La Niña set-up has a strongly negative cloud feedback, the control set-up has a negligible cloud feedback, and the El Niño set-up has a positive cloud feedback (Table 2).

The net CRE profile in the original El Niño profile has a strong minimum over the region of shallow convection ($\sim x = 7 \times 10^3$ km) which disappears with warming (Figure 12c), consistent with a positive feedback from reduced low cloudiness with warming. In the La Niña set-up, the CRE becomes more negative on the margin of the warm pool (Figure 12b), where precipitation increases most (Figure 9), connected with both an increase in cloud fraction and cloud water paths there. The net CRE also becomes more negative over the cold pool, where high cloud cover decreases with warming. In the control simulation, warming leads to a more negative CRE near the region of greatest increase in precipitation ($\sim x = 6 \times 10^3$ km), but a weakening of the negative CRE peak near ($\sim x = 9 \times 10^3$ km); these changes compensate to produce a weak cloud feedback (Figure 12a).

Although we caution against taking the feedbacks literally, the relationship we find between the SST gradient and sign of the cloud feedback – with smaller SST gradient giving a more positive cloud feedback – likely merits future investigation with mock-Walker set-ups. Our results are qualitatively consistent with inferences from AMIP models forced by historical SSTs, which typically show weaker implied climate sensitivities over the past few decades, during which the SST gradient across the equatorial Pacific has been increasing [*Andrews et al.*, 2018].

7 Conclusion

In this study, we have investigated the mean climate and response to warming of mock-Walker simulations, motivated by the need for modelling set-ups that explicitly simu-

[6] Uncertainties represent 5-95% confidence intervals, calculated using the standard error of the difference in daily-mean fluxes and with the number of degrees of freedom reduced to account for temporal autocorrelation.

late both convective systems and large-scale atmospheric flows. By prescribing a horizontally-varying SST profile, the flow in mock-Walker simulations is constrained to resemble that over the tropical Pacific, with ascent over the warm pool and subsidence over the cold pool. Our control simulation is forced by an SST profile that roughly matches the equatorial Pacific, and qualitatively reproduces many observed features, such as the zonal profiles of precipitation and the net cloud radiative effect. However, the flow in this simulation consists of two vertically-stacked cells, rather than the single cell seen in reanalysis. Simulations at colder and warmer mean SSTs indicate that the control simulation is part of a larger transition from a single overturning cell at colder SSTs to a double overturning cell at warmer SSTs, with the transition occurring near the present-day mean SST of ~300K. The upper troposphere over the cold pool of the mock-Walker simulation also shows extreme dryness (relative humidities of less than 10%) compared to reanalysis, and cloud cover is smaller than observed, leading to a weaker LW CRE and a more negative net CRE compared to satellite observations. We have been unable to find in-situ observations from the Eastern Pacific to further validate the realism of the mock-Walker simulations relative to reanalysis – which might not represent humidity or vertical velocities well in this region due to the lack of observational constraints.

The responses to mean warming in the control and La Niña simulation are largely determined by circulation changes, particularly expansion and strengthening of the lower circulation cells and contraction and weakening of the upper circulation cells. These have a large imprint on the temperature and humidity responses. The El Niño response differs from the responses in other set-ups in several notables ways, and generally appears less controlled by circulation changes. For instance, the lower troposphere moistens with warming in the El Niño set-up, but dries in the other two. The circulation also retains a similar structure and weakens modestly with warming in the El Niño simulations. All simulations show a weakening of global streamfunction maxima with warming, consistent with comprehensive climate model simulations that suggest the Walker circulation slows with warming [*Vecchi and Soden*, 2007].

Also consistent with climate model simulations, we find that the El Niño set-up, with weaker SST gradient, has a positive cloud feedback and a high climate sensitivity, whereas the La Niña set-up, with a stronger SST gradient, has a negative cloud feedback and a lower climate sensitivity. The high climate sensitivity of the El Niño set-up seems to be due to a reduction in low cloud cover over the cold pool. The weak sensitivity of the La Niña set-up seems to be associated with enhanced cloud cover on the margin of the warm pool and a reduction of cirrus cloud cover over the cold pool, though we do not understand well the mechanisms governing these changes.

In conclusion, we have found that mock-Walker simulations show both promise and limitations for studying the relationship between tropical convection and large-scale circulations. The control simulation produces a climate that resembles the observed large-scale climate of the tropics much more closely than previous RCE simulations over uniform SSTs; however, substantial differences remain, and these differences may render the model's responses to uniform and patterned warming unrealistic. The double-cell structure of the circulation, which may be related to the extreme dryness seen in the middle and upper tropospheres over the cold pools of the simulations, is particularly troubling, though we cannot rule out that Earth's Walker circulation could transition to a double-cell state at warm enough temperatures.

In Part 2 of this study we will seek to provide explanations for some of the key features seen in the simulations, including what causes the onset of a double-cell structure and why it becomes more pronounced at higher SSTs. Based on the results presented here, the prominent role of circulation change in the responses of mock-Walker simulations to warming may be a limitation on their utility for studying realistic cloud feedback, and for studying the interactions between circulations and clouds. Further study of the circulation in the mock-Walker setup is needed in order to help understand how the Earth's real Walker circulation might change with climate – either to rule out such strong circulation changes as we have found, or to determine that they are in fact physically plausible.

Acknowledgments

This work was supported by NSF grant AGS-1623218, "Collaborative Research: Using a Hierarchy of Models to Constrain the Temperature Dependence of Climate Sensitivity".

The System for Atmospheric Modeling code is available from http://rossby.msrc.sunysb.edu/~marat/SAM.html. Namelist files for all of the simulations presented here are publicly available at !!, as are pre-processing and analysis scripts required to reproduce all figures.

References

Andrews, T., and M. J. Webb (2018), The dependence of global cloud and lapse rate feedbacks on the spatial structure of tropical pacific warming, *Journal of Climate*, *31*(7), 641–654.

Andrews, T., J. M. Gregory, and M. J. Webb (2015), The dependence of radiative forcing and feedback on evolving patterns of surface temperature change in climate models., *Journal of Climate*, *28*(2), 1630–1648.

Andrews, T., J. M. Gregory, D. Paynter, L. G. Silvers, C. Zhou, T. Mauritsen, M. J. Webb, K. C. Armour, P. M. Forster, and H. Titchner (2018), Accounting for Changing Temperature Patterns Increases Historical Estimates of Climate Sensitivity, *Geophysical Research Letters*, *45*(16), 8490–8499.

Armour, K. C., C. M. Bitz, and G. H. Roe (2013), Time-Varying Climate Sensitivity from Regional Feedbacks, *Journal of Climate*, *26*, 4518–4534.

Arnold, N. P., and D. A. Randall (2015), Global-scale convective aggregation: Implications for the madden-julian oscillation, *Journal of Advances in Modeling Earth Systems*, *7*(4), 1499–1518.

Back, L. E., and C. S. Bretherton (2006), Geographic variability in the export of moist static energy and vertical motion profiles in the tropical Pacific, *Geophysical Research Letters*, *33*(17), L17,810.

Beucler, T., T. H. Abbott, T. W. Cronin, and M. S. Pritchard (2019), Comparing convective self?aggregation in idealized models to observed moist static energy variability near the equator, *Geophysical Research Letters*, *46*, 10,589–10,598.

Bony, S., B. Stevens, D. M. W. Frierson, C. Jakob, M. Kageyama, R. Pincus, T. G. Shepherd, S. C. Sherwood, A. P. Siebesma, A. H. Sobel, M. Watanabe, and M. J. Webb (2015), Clouds, circulation and climate sensitivity, *Nature Geoscience*, *8*(4), 261–268, doi:10.1038/ngeo2398.

Bretherton, C. S., and A. H. Sobel (2002), A Simple Model of a Convectively Coupled Walker Circulation Using the Weak Temperature Gradient Approximation, *Journal of Climate*, *15*, 14.

Bretherton, C. S., P. N. Blossey, and M. E. Peters (2006), Interpretation of simple and cloud-resolving simulations of moist convection-radiation interaction with a mock-Walker circulation, *Theoretical and Computational Fluid Dynamics*, *20*(5-6), 421–442, doi:10.1007/s00162-006-0029-7.

Ceppi, P., and J. M. Gregory (2017), Relationship of tropospheric stability to climate sensitivity and Earth's observed radiation budget, *Proceedings of the National Academy of Sciences*, *114*(50), 13,126–13,131.

Cess, R. D., and G. L. Potter (1988), A methodology for understanding and intercomparing atmospheric climate feedback processes in general circulation models., *Journal of Geophysical Research*, *93*, 8305–8314.

Collins, W. D., P. J. Rasch, B. A. Boville, J. J. Hack, J. R. McCaa, D. L. Williamson, B. P. Briegleg, C. M. Bitz, S. J. Lin, and M. Zhang (2006), The formulation and atmospheric simulation of the community atmosphere model version 3 (cam3)., *Journal of Climate*, *19*, 2144–2161.

Coppin, D., and S. Bony (2015), Physical mechanisms controlling the initiation of convective self-aggregation in a general circulation model, *Journal of Advances in Modeling Earth Systems*, *7*(4), 2060–2078.

Cronin, T. W. (2014), On the Choice of Average Solar Zenith Angle, *Journal of the Atmospheric Sciences*, *71*(8), 2994–3003.

Cronin, T. W., and A. A. Wing (2017), Clouds, circulation, and climate sensitivity in a radiative-convective equilibrium channel model., *Journal of Advances in Modeling Earth Systems*, *9*(5), 2883–2905.

Dee, D. P., S. M. Uppala, A. J. Simmons, P. Berrisford, P. Poli, S. Kobayashi, U. Andrae, M. A. Balmaseda, G. Balsamo, P. Bauer, P. Bechtold, A. C. M. Beljaars, L. v. d. Berg, J. Bidlot, N. Bormann, C. Delsol, R. Dragani, M. Fuentes, A. J. Geer, L. Haimberger, S. B. Healy, H. Hersbach, E. V. HÃşlm, L. Isaksen, P. KÃěllberg, M. KÃűhler, M. Matricardi, A. P. McNally, B. M. MongeâĂŘSanz, J.-J. Morcrette, B.-K. Park, C. Peubey, P. d. Rosnay, C. Tavolato, J.-N. ThÃľpaut, and F. Vitart (2011), The ERA-Interim reanalysis: configuration and performance of the data assimilation system, *Quarterly Journal of the Royal Meteorological Society*, *137*(656), 553–597.

Dong, Y., C. Proistosescu, K. C. Armour, and D. S. Battisti (2019), Attributing Historical and Future Evolution of Radiative Feedbacks to Regional Warming Patterns using a Green's Function Approach: The Preeminence of the Western Pacific, *Journal of Climate*, *32*(17), 5471–5491.

Emanuel, K. (2019), Inferences from Simple Models of Slow, Convectively Coupled Processes, *Journal of the Atmospheric Sciences*, *76*(1), 195–208.

Forster, P. M., T. Andrews, P. Good, J. M. Gregory, L. S. Jackson, and M. Zelinka (2013), Evaluating adjusted forcing and model spread for historical and future scenarios in the cmip5 generation of climate models, *Journal of Geophysical Research: Atmospheres*, *118*, 1139–1150.

Grabowski, W., and M. Moncrieff (2001), Large-scale organization of tropical convection in two-dimensional explicit numerical simulations, *Q. J. R. Meteorol. Soc.*, *127*, 445–468.

Grabowski, W., and M. Moncrieff (2002), Large-scale organization of tropical convection in two-dimensional explicit numerical simulations: Effects of interactive radiation, *Q. J. R. Meteorol. Soc.*, *128*, 2349–2375.

Grabowski, W. W., J.-I. Yano, and M. W. Moncrieff (2000), Cloud resolving modeling of tropical circulations driven by large-scale sst gradients, *Journal of the Atmospheric Sciences*, *57*(23), 2022–2039.

Harrop, B. E., and D. L. Hartmann (2016), The role of cloud radiative heating within the atmosphere on the high cloud amount and top-of-atmosphere cloud radiative effect, *Journal of Advances in Modeling Earth Systems*, *8*(23), 1391–1410.

Holloway, C. E., A. A. Wing, S. Bony, C. Muller, H. Masunaga, T. S. L'Ecuyer, D. D. Turner, and P. Zuidema (2017), Observing convective aggregation, *Surveys of Geophysics*, *38*, 1199–1236.

Inoue, K., and L. E. Back (2015), Gross Moist Stability Assessment during TOGA COARE: Various Interpretations of Gross Moist Stability, *Journal of the Atmospheric Sciences*, *72*(11), 4148–4166.

Khairoutdinov, M. F., and D. A. Randall (2003), Cloud resolving modeling of the arm summer 1997 iop: Model formulation, results, uncertainties, and sensitivities, *Journal of the Atmospheric Sciences*, *60*(23), 607–625.

Kuang, Z. (2012), Weakly Forced Mock Walker Cells, *Journal of the Atmospheric Sciences*, *69*(9), 2759–2786.

Larson, K., and D. L. Hartmann (2003), Interactions among cloud, water vapor, radiation, and large-scale circulation in the tropical climate. part ii: Sensitivity to spatial gradients of sea surface temperature., *Journal of Climate*, *16*(10), 1441–1455.

Lindzen, R. S., and S. Nigam (1987), On the role of sea surface temperature gradients in forcing low level winds and convergence in the tropics, *Journal of the Atmospheric Sciences*, *44*(23), 2418–2436.

Liu, C., and M. W. Moncrieff (2008), Explicitly simulated tropical convection over idealized warm pools, *Journal of Geophysical Research: Atmospheres*, *113*(D21).

Lloyd, J., E. Guilyardi, and H. Weller (2012), The Role of Atmosphere Feedbacks during ENSO in the CMIP3 Models. Part III: The Shortwave Flux Feedback, *Journal of Climate*, *25*(12), 4275–4293.

Lutsko, N. J. (2018), The Relationship Between Cloud Radiative Effect and Surface Temperature Variability at El Niño-Southern Oscillation Frequencies in CMIP5 Models, *Geophysical Research Letters*, *45*(19), 10,599–10,608, doi:10.1029/2018GL079236.

Lutsko, N. J., and T. W. Cronin (2018), Increase in Precipitation Efficiency With Surface Warming in Radiative-Convective Equilibrium, *Journal of Advances in Modeling Earth Systems*, *10*(11), 2992–3010, doi:10.1029/2018MS001482.

Meraner, K., T. Mauritsen, and A. Voigt (2013), Robust increase in equilibrium climate sensitivity under global warming, *Geophysical Research Letters*, *40*(22), 5944–5948.

Merlis, T. M., and T. Schneider (2011), Changes in zonal surface temperature gradients and walker circulations in a wide range of climates, *Journal of Climate*, *24*(17), 4757–4768.

Muller, C. J., and I. M. Held (2012), Detailed Investigation of the Self-Aggregation of Convection in Cloud-Resolving Simulations, *Journal of the Atmospheric Sciences*, *69*(8), 2551–2565, doi:10.1175/JAS-D-11-0257.1.

Muller, C. J., P. A. OâĂŹGorman, and L. E. Back (2011), Intensification of Precipitation Extremes with Warming in a Cloud-Resolving Model, *Journal of Climate*, *24*(11), 2784–2800, doi:10.1175/2011JCLI3876.1.

Park, S., and C. B. Leovy (2004), Marine Low-Cloud Anomalies Associated with ENSO, *JOURNAL OF CLIMATE*, *17*, 22.

Pendergrass, A. G., K. A. Reed, and B. Medeiros (2016), The link between extreme precipitation and convective organization in a warming climate: Global radiative-convective equilibrium simulations, *Geophysical Research Letters*, *43*(21), 11,445–11,452.

Peters, M. E., and C. S. Bretherton (2005), A Simplified Model of the Walker Circulation with an Interactive Ocean Mixed Layer and Cloud-Radiative Feedbacks, *Journal of Climate*, *18*(20), 4216–4234.

Posselt, D. J., S. C. v. d. Heever, and G. L. Stephens (2008), Trimodal cloudiness and tropical stable layers in simulations of radiative convective equilibrium, *Geophysical Research Letters*, *35*(8).

Posselt, D. J., S. v. d. Heever, G. Stephens, and M. R. Igel (2012), Changes in the Interaction between Tropical Convection, Radiation, and the Large-Scale Circulation in a Warming Environment, *Journal of Climate*, *25*(2), 557–571.

Randall, D., M. Khairoutdinov, A. Arakawa, and W. Grabowski (2003), Breaking the Cloud Parameterization Deadlock, *Bulletin of the American Meteorological Society*, *84*(11), 1547–1564, doi:10.1175/BAMS-84-11-1547.

Reed, K. A., B. Medeiros, J. T. Bacmeister, and P. H. Lauritzen (2015), Global radiativeâĂŞconvective equilibrium in the community atmosphere model, version 5, *Journal of the Atmospheric Sciences*, *72*(15), 2183–2187.

Romps, D. M. (2014), An analytical model for tropical relative humidity., *Journal of Climate*, *27*(23), 7432–7449.

Schneider, T., J. Teixeira, C. S. Bretherton, F. Brient, K. G. Pressel, C. SchÃďr, and A. P. Siebesma (2017), Climate goals and computing the future of clouds, *Nature Climate Change*, *7*(1), 3–5, doi:10.1038/nclimate3190.

Schwendike, J., P. Govekar, M. J. Reeder, R. Wardle, G. J. Berry, and C. Jakob (2014), Local partitioning of the overturning circulation in the tropics and the connection to the Hadley and Walker circulations, *Journal of Geophysical Research: Atmospheres*, *119*(3), 1322–1339.

Seeley, J. T., and D. M. Romps (2015), Why does tropical convective available potential energy (CAPE) increase with warming?, *Geophysical Research Letters*, *42*(23), 10,429–10,437, doi:10.1002/2015GL066199.

Silvers, L. G., D. Paynter, and M. Zhao (2018), The diversity of cloud responses to twentieth century sea surface temperatures, *Geophysical Research Letters*, *45*(1), 391–400, 2017GL075583.

Singh, M. S., and P. A. O'Gorman (2013), Influence of entrainment on the thermal stratification in simulations of radiative-convective equilibrium, *Geophysical Research Letters*, *40*(16), 4398–4403, doi:10.1002/grl.50796.

Slawinska, J., O. Pauluis, A. J. Majda, and W. W. Graboskwi (2014), Multiscale interactions in an idealized walker circulation: Mean circulation and intraseasonal variability, *Journal of the Atmospheric Sciences*, *71*(3), 953–971.

Soden, B. J., and I. M. Held (2006), An assessment of climate feedbacks in coupled ocean-atmosphere models, *Journal of Climate*, *19*(6), 3354–3360.

Stephens, G. L., S. van den Heever, and L. Pakula (2008), RadiativeâĂŞConvective Feedbacks in Idealized States of RadiativeâĂŞConvective Equilibrium, *Journal of the Atmospheric Sciences*, *65*(12), 3899–3916.

Stevens, B., and S. Bony (2013), What Are Climate Models Missing?, *Science*, *340*(6136), 1053–1054, doi:10.1126/science.1237554.

Tompkins, A. M., and G. C. Craig (1998), Radiative-convective equilibrium in a three-dimensional cloud-ensemble model, *Quarterly Journal of the Royal Meteorological Society*, *124*(23), 2073–2097.

Vecchi, G. A., and B. J. Soden (2007), Global Warming and the Weakening of the Tropical Circulation, *Journal of Climate*, *20*(17), 4316–4340.

Vial, J., J.-L. Dufreshne, and S. Bony (2013), On the interpretation of inter-model spread in cmip5 climate sensitivity estimates., *Climate Dynamics*, *41*(1), 3339–3362.

Wing, A. A. (2019), Self-aggregation of deep convection and its implications for climate, *Current Climate Change Reports*, *5*(2), 1–11.

Wing, A. A., and T. W. Cronin (2016), Self aggregation in long channel geometry., *Quarterly Journal of the Royal Meteorological Society*, *142*(5), 1–15.

Wing, A. A., and K. A. Emanuel (2014), Physical mechanisms controlling self-aggregation of convection in idealized numerical modeling simulations, *Journal of Advances in Modeling Earth Systems*, *6*(1), 59–74, doi:10.1002/2013MS000269.

Wing, A. A., K. A. Reed, M. Satoh, B. Stevens, S. Bony, and T. Ohno (2018), Radiative-convective equilibrium model intercomparison project, *Geoscientific Model Development*, *11*(2), 793–813.

Wofsy, J., and Z. Kuang (2012), Cloud-resolving model simulations and a simple model of an idealized walker cell, *Journal of Climate*, *25*(10), 8090–8106.

Yano, J.-I., W. W. Grabowski, and M. W. Moncrieff (2002a), Mean-state convective circulations over large-scale tropical sst gradients, *Journal of the Atmospheric Sciences*, *59*(23), 1578–1592.

Yano, J.-I., M. W. Moncrieff, and W. W. Grabowski (2002b), Walker-Type Mean Circulations and Convectively Coupled Tropical Waves as an Interacting System, *Journal of the Atmospheric Sciences*, *59*, 1566–1577.

Zhou, C., M. D. Zelinka, and S. A. Klein (2017), Analyzing the dependence of global cloud feedback on the spatial pattern of sea surface temperature change with a green's function approach, *Journal of Advances in Modeling Earth Systems*, *9*(23), 2174–2189.

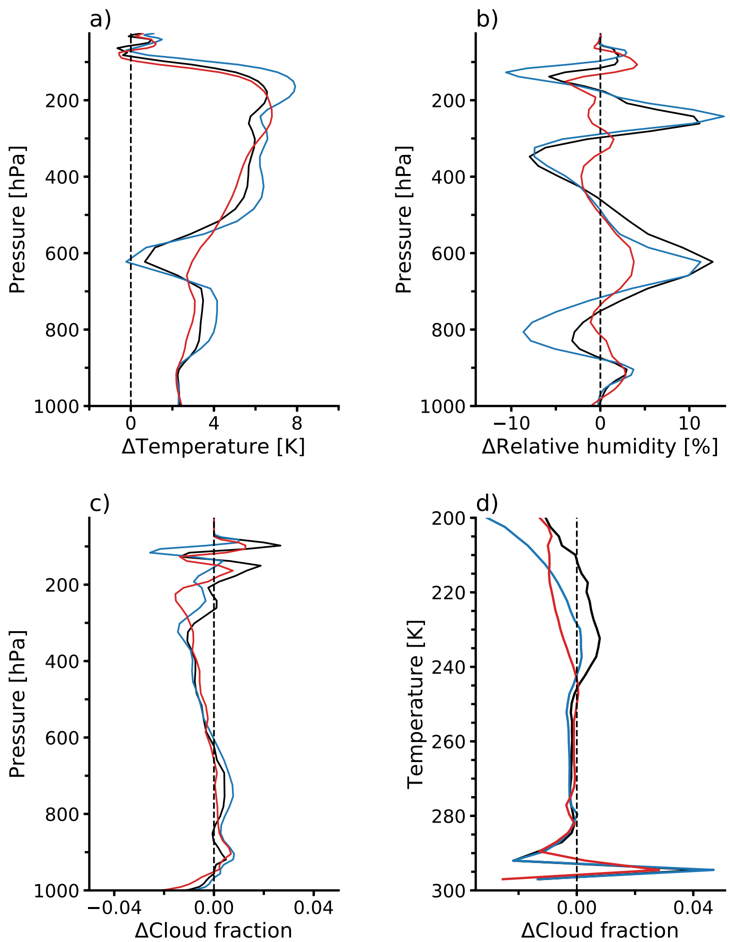

Figure 10. a) Response of horizontal-mean temperature to increasing the mean SST by 2K with the control SST gradient (black curve), with the enhanced La Niña gradient (blue curve) and with the reduced La Niña gradient (red curve). b) Same as a) but for the relative humidity. c) Same as a) but for the cloud fraction. d) Same as c) but the cloud fraction changes are plotted versus the horizontal-mean temperature profiles in the 300.5K simulations (the cloud cover profiles in the +2K simulations are linearly interpolated onto the 300.5K temperature grids, with values at warmer temperatures discarded).

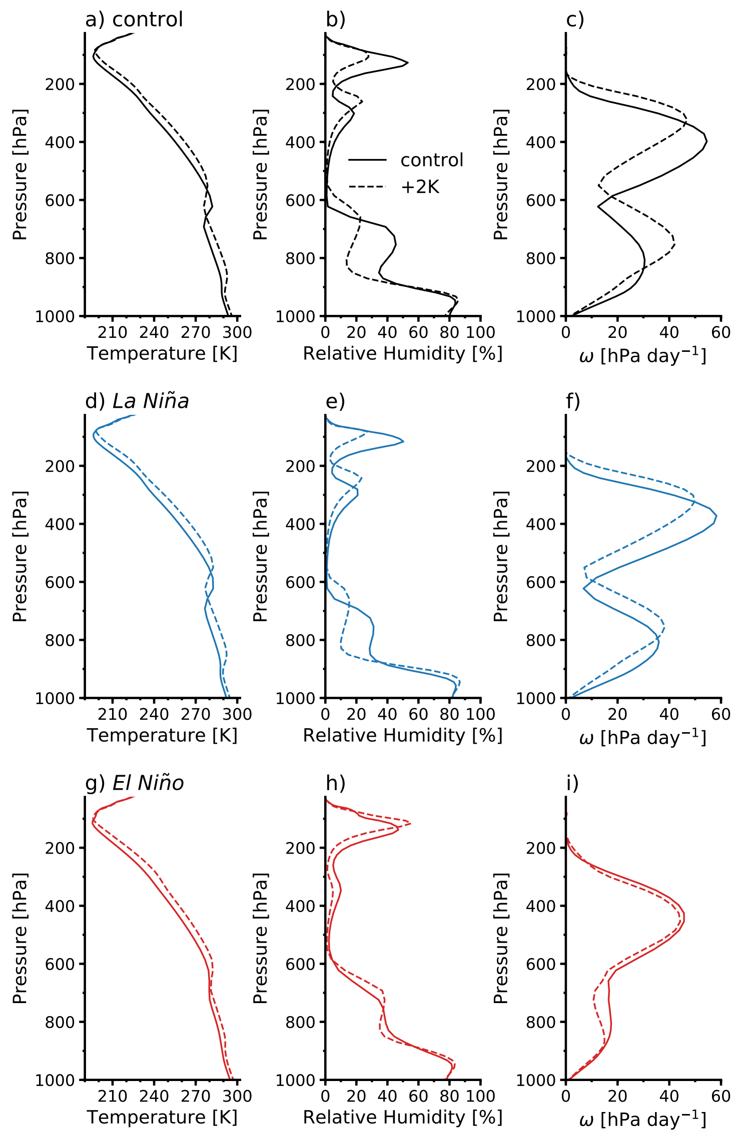

Figure 11. a) Average temperature profiles in the cold pool regions (x = 10-12×10^3km) of the control mock-Walker simulation (solid black line), and of the +2K simulation with the control SST gradient (dashed black line). b) Average relative humidity profiles in the cold pool regions of the same simulations. c) Average vertical pressure velocity profiles in the cold pool regions of the same simulations.

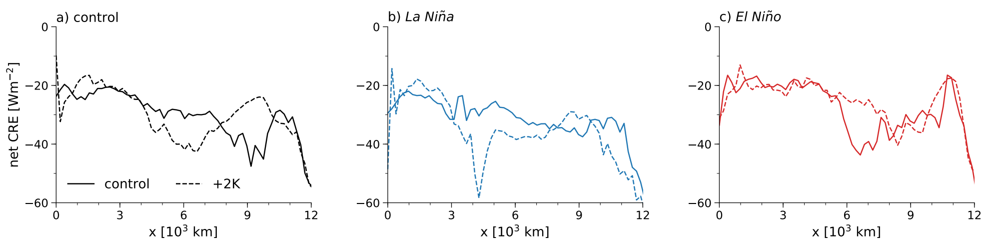

Figure 12. a) Profiles of net CRE in the control mock-Walker simulation (solid curve) and the +2K simulation (dashed curve). b) Same as panel a) but for the simulations with enhanced SST gradient. c) Same as panel a) but for the simulations with reduced SST gradient.